



CHORUS

This is the accepted manuscript made available via CHORUS. The article has been published as:

Large Fermi surface expansion through anisotropic mixing of conduction and f electrons in the semimetallic Kondo lattice CeBi

Peng Li, Zhongzheng Wu, Fan Wu, Chunyu Guo, Yi Liu, Haijiang Liu, Zhe Sun, Ming Shi, Fanny Rodolakis, Jessica L. McChesney, Chao Cao, Huiqiu Yuan, Frank Steglich, and Yang Liu

Phys. Rev. B **100**, 155110 — Published 7 October 2019

DOI: [10.1103/PhysRevB.100.155110](https://doi.org/10.1103/PhysRevB.100.155110)

Large Fermi Surface Expansion through Anisotropic Mixing of Conduction- and f -electrons in the Semimetallic Kondo Lattice CeBi

**Peng Li¹, Zhongzheng Wu¹, Fan Wu¹, Chunyu Guo¹, Yi Liu², Haijiang Liu³, Zhe Sun²,
Ming Shi³, Fanny Rodolakis⁴, Jessica L McChesney⁴, Chao Cao⁵, Huiqiu Yuan^{1,6,7*}, Frank
Steglich^{1*}, and Yang Liu^{1,6,7*}**

¹Center for Correlated Matter and Department of Physics, Zhejiang University, Hangzhou, P. R.
China

²National Synchrotron Radiation Laboratory, University of Science and Technology of China,
Hefei, P. R. China

³Paul Scherrer Institute, Swiss Light Source, CH-5232 Villigen PSI, Switzerland

⁴Advanced Photon Source, Argonne National Lab, 9700 South Cass Avenue, Argonne, Illinois
60439, USA

⁵Department of Physics, Hangzhou Normal University, Hangzhou, P. R. China

⁶Zhejiang Province Key Laboratory of Quantum Technology and Device, Zhejiang University,
Hangzhou, P. R. China

⁷Collaborative Innovation Center of Advanced Microstructures, Nanjing University, Nanjing,
China

*Corresponding authors: yangliuphys@zju.edu.cn, Frank.Steglich@cpfs.mpg.de,
hqyuan@zju.edu.cn

Abstract

Using angle-resolved photoemission spectroscopy (ARPES) and resonant ARPES, we report evidence of strong anisotropic conduction- f electron mixing (c - f mixing) in CeBi by observing a largely expanded Ce- $5d$ pocket at low temperature, with no change in the Bi- $6p$ bands. The anisotropic Fermi surface (FS) expansion is accompanied by a pronounced spectral weight transfer from the local $4f^0$ peak of Ce (corresponding to Ce^{3+}) to the itinerant conduction bands near the Fermi level. Careful analysis suggests that the observed large FS change (with a volume expansion of the electron pocket up to 40%) can most naturally be explained by a small valence change ($\sim 1\%$) of Ce, which coexists with a very weak Kondo screening. Our work therefore provides evidence for a FS change driven by real charge fluctuations deep in the Kondo limit, which is highly dependent on the orbital character and momentum and is made possible by the low carrier density.

1. Introduction

Intermetallic compounds of some rare earths (RE, notably Ce and Yb) frequently behave as Kondo-lattice (KL) systems. Well below the Kondo temperature T_K , they can develop different types of interesting ground-state properties, including heavy Fermi-liquid, unconventional superconducting, magnetically ordered, or Kondo insulating/semi-metallic phases [1,2,3,4,5]. For these materials, T_K may vary between a few K (“Kondo limit”) and a few hundred K (“Intermediate Valence (IV) limit”). In the Kondo limit, Kondo screening of the local $4f$ -moments plays the key role over a wide temperature range up to above T_K . This is a many-body process involving the local $4f$ -electron states and electron-hole pairs at the Fermi level (E_F), leading to spin flips without changing the $4f$ -occupation (“virtual charge fluctuations”). Meanwhile, there exists a minority of “real charge (valence) fluctuations” due to the weak (covalent) mixing or hybridization, which is necessary for the Kondo screening to operate, as described by the periodic Anderson model [6]. Therefore, for KL systems, the Ce valence is not exactly integer (typically $3 < \nu < 3.1$) and increases slightly upon cooling. In the IV limit, where ν is typically between 3.2 and 3.5, the valence fluctuations predominate, but the Kondo spin flips are still operating. This is illustrated by the negative temperature coefficient (NTC) of the resistivity, $\rho(T) \sim -\log T/T_K$, in the canonical IV compound CePd₃ [7]. On the other hand, it was found for dilute IV Eu ions in ScAl₂ in the absence of Kondo spin flips that the incremental Eu-derived resistivity exhibits a positive T -coefficient [8], while a Kondo-type NTC is observed for a few Eu-based compounds [9]. It is therefore a big challenge to resolve valence fluctuations from Kondo spin flips, particularly for KL systems with low T_K , where the Kondo screening is predominant, and the effect of tiny valence fluctuations is almost impossible to identify unambiguously in transport and thermodynamic measurements.

As will be shown below, low carrier density KL systems provide an interesting case to resolve valence-fluctuation-induced changes in the Fermi surface (FS), deep in the Kondo limit. The low carrier density significantly reduces the Kondo screening, while the small FS allows for easy detection of any change in the Fermi wavevector k_F due to valence fluctuations. Low carrier density Kondo systems have attracted considerable interest recently, in view of novel phenomena such as unconventional quantum criticality and correlated topological states [10,11,12,13,14]. This has motivated us to study CeBi, a well-known low carrier density KL system (~ 0.03 e⁻/Ce [15]). CeBi was extensively studied in the past because of its anomalous electromagnetic properties [16,17,18,19,20,21]. Its resistivity shows NTC suggesting Kondo screening, with a very low T_K due to the few carriers available. As a consequence, the $4f$ -moments are only very weakly screened and undergo antiferromagnetic (AFM) order at $T_{N1} \simeq 25$ K and $T_{N2} \simeq 12$ K, respectively [16,22]. According to Kasuya and collaborators [17,23], the weak Kondo interaction becomes substantially strengthened by the strong mixing between the Bi- $6p$ and Ce- $4f$ states (p - f mixing). An alternative proposal, however, has argued for non-Kondo exchange to explain the electromagnetic properties [18]. The band structure of CeBi was studied previously by ARPES [14,19], revealing the coexistence of hole and electron bands near E_F , but the low temperature properties, particularly the role of $4f$ electrons, were not addressed.

2. Experimental and Computational Details

ARPES measurements of single-crystal CeBi (with a typical size of $\sim 1 \times 1$ mm) were performed at low temperatures (from 10 K to ~ 70 K), after being cleaved *in-situ* at low temperatures with a base pressure $< 1 \times 10^{-10}$ Torr. Off-resonant ultraviolet ARPES measurements ($h\nu < 40$ eV) were carried out at the BL13U beamline in National Synchrotron Radiation Lab

(NSRL, Hefei). The Fermi surface (FS) maps are obtained using a DA30 electron analyzer with deflector scanning mode. On-resonant ARPES measurements near the Ce N (~ 122 eV) edge were performed at the SIS beamline at the Swiss Light Source, Villigen. In order to probe the intrinsic bulk electronic structure, soft X-ray resonant ARPES measurements were also performed near the Ce M edge (~ 880 eV) at the 29-ID IEX beamline at the Advanced Photon Source, Argonne. The typical energy (momentum) resolution is ~ 15 meV (~ 0.01 \AA^{-1}) for both the ultraviolet off-resonant and the N edge resonant ARPES, while the energy (momentum) resolution is ~ 100 meV (~ 0.03 \AA^{-1}) for the M edge resonant ARPES. The much reduced energy/momentum resolution in the M edge resonant ARPES is due to the large photon (and hence photoelectron) energy, which imposes technical challenges in these measurements. Nevertheless, the M edge resonant ARPES measurement is much more bulk-sensitive and predominantly probes the bulk Ce $4f$ electrons, which provides important orbital-specific information. All data presented in this paper were taken only within a few hours after the low-temperature cleave (typically < 5 hours), to ensure that our results are not affected by sample aging.

Electronic structure calculations in this paper were performed using density functional theory (DFT) and a plane-wave basis projected augmented wave method, as implemented in the Vienna Ab Initio Simulation Package (VASP) [24]. f electrons have been treated as core electrons and spin-orbit coupling is taken into account in the calculations [25]. We have employed the modified Becke-Johnson (MBJ) potential to obtain good agreement with experiments [26,27]. The spectral calculations in Fig. 1(b,c) are obtained from surface Green's function (GF) method using Hamiltonian from DFT calculations [25]. This method integrates the

states from semi-infinite layers and the surface. Numerically, the infinitesimal imaginary number was chosen to be $\eta=0.001$ eV to ensure causality in the retarded GF.

3. Results and Discussion

3.1. Band Structure and Fermi Surface Expansion

Bulk CeBi crystallizes in the simple rock-salt structure; its three-dimensional (3D) Brillouin zone (BZ) and associated two-dimensional (2D) BZ are shown in Fig. 1(a). At high temperature, the Ce has a valence close to +3 (with one $4f$ electron), and the FS consists of two small hole pockets at the Γ point (from Bi- $6p$ orbitals) and one small electron pocket at each symmetry-equivalent X point (from Ce- $5d$ orbitals) [14,27]. All states contributing to the FS are bulk states. The bottom panel in Fig. 1(a) displays the 3D bulk FS from density-functional theory (DFT) calculations, assuming the $4f$ electrons to be completely localized [25,27]. The experimental FSs near the 2D $\bar{\Gamma}$ and \bar{M} points (the X point in 3D bulk BZ projects onto the \bar{M} point in 2D BZ), obtained by ARPES measurements at both 10 K and ~ 37 K, are displayed in Fig. 1(b,c), in comparison with the k_z projected DFT calculations. Good overall agreements between the experiments and calculations can be found, implying that the $4f$ electrons remain almost fully localized (hence excluded from the FS) even down to ~ 10 K.

Assuming completely localized $4f$ electrons, the Luttinger volume of the hole pockets (Bi $6p$) should be the same as that of the electron pockets (Ce $5d$), as required by the charge neutralization. However, we observe experimentally that the electron pocket near the \bar{M} point expands considerably at lower temperatures, while the hole pockets near the $\bar{\Gamma}$ point remain unchanged (see momentum-distribution curves (MDCs) in Fig. 1(d,e) and energy-momentum cuts in Fig. 2(a,b)). Our detailed analysis indicates that the electron pocket expands mainly along

the short axis (Fig. 1(e)), which results in a volume increase of $\sim 40\%$ at ~ 10 K compared to that at ~ 37 K, while no change can be detected for the hole pocket. This temperature dependence is confirmed by measurements from different samples (>10). The imbalanced change of hole and electron pockets implies that additional electrons (other than Bi-6*p* and Ce-5*d*) become involved in the FS at low temperature.

3.2. Temperature Evolution of the Electron Pocket

The temperature evolution of k_F for the electron pocket is summarized in Fig. 2(c), where the top panel shows the raw data from one representative sample, demonstrating the onset temperature of ~ 35 K for the pocket expansion. To account for slight variations in k_F for different samples and highlight the temperature evolution, we normalize the k_F with respect to its high temperature value, i.e., $k_F(T) / k_F(T > 35 \text{ K})$, and plot it at the bottom panel for four different samples. The result clearly shows that the pocket gradually expands with decreasing temperature and eventually reaches a plateau near 10 K. Since CeBi develops AFM order at ~ 25 K, the observed FS expansion might be related to the AFM transition. However, neither the FS maps in Fig. 1 nor the energy-momentum cuts in Fig. 2(a,b) show any sign of band folding at low temperature (more data can be found in [28]), indicating that the band folding effect from AFM ordering is very weak and does not play a significant role here. We also performed similar ARPES measurements for GdBi (Fig. 2(d)), an isostructural compound with AFM ordering at 25 K; the results show no temperature dependence for both the hole and electron pockets, in sharp contrast to CeBi (see [28] for additional data and analysis). In contrast to the ‘unstable’ 4*f* shell of CeBi with 4*f* occupancy $n_f \leq 1$, the half-filled one ($n_f = 7$) of GdBi is very ‘stable’. Therefore, the observed expansion of the electron pocket in CeBi should most naturally be associated with

the Ce-derived $4f$ electrons. This is also supported by the comparison of $\rho(T)$ in Fig. 2(e): while the resistivity of CeBi exhibits a clear Kondo-type upturn from high temperature to ~ 25 K and a sharp decrease below 25 K, the resistivity of GdBi shows only a tiny kink at the AFM transition, without any sign of Kondo-like behavior. For CeBi, the incremental resistivity, obtained after subtracting the result for LaBi ($\rho_i = \rho_{\text{CeBi}} - \rho_{\text{LaBi}}$), indeed follows the logarithmic temperature dependence characteristic for Kondo scattering (inset of Fig. 2(e)).

3.3. Temperature-dependent Spectral Weight Transfer in Resonant ARPES

To better understand the Kondo effect and c - f mixing, we performed resonant ARPES measurements at Ce N edge ($4d \rightarrow 4f$) to enhance the spectral contribution from $4f$ electrons (Fig. 3(a)). We can clearly observe a sharp dispersionless $4f^0$ peak at ~ -2.8 eV and the $4f^1$ peak at -0.3 eV, respectively. Here the labels, $4f^0$ and $4f^1$, refer to the electronic configuration after photoexcitation – therefore the $4f^0$ and $4f^1$ peak corresponds to the localized $4f$ electron (Ce^{3+}) and the many-body Kondo resonance (KR), respectively. The $4f^1$ peak at -0.3 eV is actually the spin-orbit split satellite (angular momentum $J=7/2$) of the KR, while the $J=5/2$ KR peak near E_F is quite weak and almost absent (see Fig. 2(b) and Fig. 3(a)), similar to CeSb [29]. The presence of the $J=7/2$ peak implies that the Kondo process is indeed active, and the rather weak $J=5/2$ peak indicates that its T_K must be very low [30,31]. The small T_K is well expected for a low carrier density KL system, as the strength of the Kondo screening is strongly dependent on the density of conduction electrons [1].

Fig. 3(a) also shows the comparison of energy distribution curves (EDCs) near the hole and electron pockets at 16 K and 35 K, respectively. A very small decrease of the $4f^0$ peak intensity and a slight increase of the conduction bands near the $J=7/2$ $4f^1$ peak are seen at lower

temperature. This trend becomes much clearer for soft X-ray resonant ARPES measurements at Ce M edge (Fig. 3(b,c)), which is more bulk-sensitive due to higher energies. Below resonance (875 eV), the APRES spectra are dominated by the non- f conduction bands, whose EDCs exhibit no temperature dependence (Fig. 3(c)). Upon cooling at resonance, e.g., at 880.6 eV and 881.2 eV, one can clearly observe a pronounced decrease of the $4f^0$ peak and a simultaneous intensity increase of the conduction bands from E_F to ~ -1.5 eV. Additional data from another sample with a cooling and warming cycle is shown in [28]. Here the conduction bands are not resolved as clearly as those in Fig. 1 and Fig. 2, likely due to the limited resolution and low counts in soft X-ray ARPES. The pronounced temperature-dependent intensity transfer in Fig. 3(c) represents a direct evidence for the strong c - f mixing at low temperature, which couples the wavefunctions of conduction and f electrons, resulting in higher f weight near E_F (itinerant) and lower f weight at $4f^0$ (localized) with decreasing temperature.

3.4. Valence-induced Fermi Surface Change

Our observation that both the spectral weight transfer in Fig. 3(c) and the FS expansion in Fig. 2(c) onset at $\simeq 35$ K indicates that these two phenomena are intimately connected. According to Luttinger's theorem, the transfer of (a small amount of localized) $4f$ electrons into the conduction bands can lead to an expanded FS. Note that the FS change seen here is different from the small-to-large FS change observed in heavy fermion (HF) metals upon cooling [32,33,34,35,36], during which a strong and coherent KR develops near E_F and hybridizes with the conduction bands, resulting in an increased k_F . Figure 4(a) shows the zoom-in view of the ARPES spectra near E_F . It is clear that the $J=5/2$ KR is extremely weak (if any), and therefore there must be a different cause for the FS expansion. In fact, Fig. 2(a) shows that the electron

pocket expansion is accompanied by a downward shift of the whole Ce-5*d* band in energy. This behavior can be most naturally explained by a slight increase of Ce valence on cooling from ~ 35 to ~ 10 K, which we estimate to be ~ 0.01 based on the Luttinger count of the observed electron pocket. As stated in the introduction, such temperature dependence of the RE valence in KL systems appears to be quite natural [6,37,38]. In low carrier density systems, the many-body Kondo effect is largely diminished due to the stringent requirement for the conduction electron density and, therefore, the valence fluctuation originating in the substantial *c-f* mixing can be resolved via the FS expansion. Such a small valence-induced change in FS is difficult to resolve in metallic KL systems, but it can be identified in low carrier density KL systems.

The valence-induced pocket expansion is mainly along the short axis of the ellipse (Fig. 1(e)), demonstrating that the *c-f* mixing is highly anisotropic in momentum space. While we do not have a good quantitative explanation yet, this is likely related to the hybridization matrix element involving the detailed wave function of Ce-4*f* and conduction electrons. In addition to the downward shift of the Ce-5*d* band near E_F at the \overline{M} point (Fig. 2(a)), we also observe similar shift of the bands at deeper binding energies at low temperature (see [28] for detailed EDC analysis). These deeper bands contain contributions from Ce-5*d* orbitals as well, although mixing with Bi-6*p* orbitals is also present due to band overlapping [27]. These bands can therefore shift towards lower energies as a result of the Ce valence change.

The observed intensity decrease of the $4f^0$ peak in Fig. 3(c) is much larger than the estimated valence increase of ~ 0.01 based on the Luttinger count of the electron pocket. This indicates that the observed spectral weight transfer in Fig. 3(c) should not be interpreted as being directly proportional to the actual number of transferred electrons. Instead, since the resonant ARPES intensity is proportional to the product of the electronic spectral function and the

photoemission matrix element from the f component (due to the resonance condition), the spectral weight transfer in Fig. 3(c) should contain a large contribution from the variation of matrix element, i.e., the reduced (increased) f component in the wave function of $4f^0$ state (conduction bands) upon cooling.

The proposed p - f mixing between the Bi- $6p$ and Ce- $4f$ states apparently does not change much within the measurement temperature window in CeBi [17], as evidenced by the weak $J=5/2$ KR and the lack of any resolvable change in the Bi $6p$ band (see Fig. 4(b,c)). On the other hand, the large temperature-dependent expansion of the Ce $5d$ band can be explained by a tiny increase of the Ce valence (~ 0.01), which could be checked by ultrahigh-resolution XAS at Ce L -edge in the future [39,40]. The expansion of Ce $5d$ pocket provides evidence for a strong covalent d - f mixing among neighboring Ce ions, which contributes to the observed spectral transfer from the localized Ce- $4f$ states into itinerant Ce- $5d$ bands near E_F , i.e., the action of valence fluctuations. It is interesting to compare our results on CeBi with those of CeSb, where a recent ARPES study also revealed two different channels of interactions by the Ce- $4f$ electrons [29], i.e., the Kondo interaction (related to p - f mixing) and magnetic exchange interaction (via d - f mixing). We make the interesting observation that the d - f mixing is obviously stronger in CeBi, compared to CeSb, with no sign of magnetic exchange splitting [29]. This difference is likely related to differences in the lattice constants and/or charge carrier densities.

4. Conclusions

To summarize, we have experimentally observed a large expansion (by $\sim 40\%$) of the Ce- $5d$ pocket in CeBi at low temperature, while the Bi- $6p$ pockets remain unchanged. Resonant ARPES measurements at low temperature revealed pronounced spectral weight transfer from the

$4f^0$ state into the conduction bands near E_F , sharing similar temperature dependence with the FS expansion. The $J=7/2$ satellite of the KR could be clearly resolved, implying that the Kondo screening is operating, although a weak $J=5/2$ KR at E_F indicates very low T_K . The observed FS expansion, distinct from the small-to-large FS change in metallic KL systems, can be explained by a small valence change of Ce (~ 0.01). Such valence-induced FS expansion goes beyond a simple rigid band shift. Rather, it is highly anisotropic in momentum space, due to an anisotropic c - f mixing; there is strong momentum-dependent hybridization of the Ce- $4f$ electrons with the $5d$ electrons of neighboring Ce ions, but an only very weak one with the Bi- $6p$ electrons. Our study demonstrates that weak valence fluctuations can be made visible in low-carrier density KL systems via significant thermally-driven changes in the FS, which can be important to understand relevant physical properties. The observed concurrence of real and virtual charge fluctuations as well as local-moment AFM order describes a state of quantum matter which has been enigmatic for years and deserves further scrutiny by future studies.

Acknowledgments

This work is supported by National Key R&D Program of the MOST of China (Grant No. 2017YFA0303100, 2016YFA0300203), National Science Foundation of China (No. 11674280, No. 11274006) and the Fundamental Research Funds for the Central Universities (2019QNA3007). We would like to thank Pengdong Wang, Dr. Caizhi Xu, Dr. Junzhang Ma for help in the synchrotron ARPES measurements. Y. L. thanks Profs. Qimiao Si and Stefan Kirchner for enlightening discussions. The synchrotron ARPES measurements was performed at BL13U beamline in Hefei national synchrotron radiation lab, SIS beamline at Swiss Light Source and 29-ID IEX beamline at Advanced Photon Source (APS). APS is supported by U.S.

Department of Energy (DOE) Office of Science under Contract No. DE-AC02-06CH11357; additional support by National Science Foundation under Grant no. DMR-0703406 is also acknowledged.

Reference

- [1] P. Coleman, *Heavy Fermions: electrons at the edge of magnetism*. Handbook of Magnetism and Advanced Magnetic Materials, vol. 1 (Wiley, New York, 2007).
- [2] H. Löhneysen, A. Rosch, M. Vojta, and P. Wolfle, *Rev. Mod. Phys.* **79**, 1015 (2007).
- [3] Q. Si and F. Steglich, *Science* **329**, 1161 (2010).
- [4] F. Steglich, J. Aarts, CD. Bredl, W. Lieke, D. Meschede, W. Franz, and H. Schäfer, *Phys. Rev. Lett.* **43**, 1892 (1979).
- [5] H. Q. Yuan, F. M. Grosche, M. Deppe, C. Geibel, G. Sparn and F. Steglich, *Science* **302**, 2104 (2003).
- [6] A. C. Hewson, *The Kondo Problem to Heavy Fermions*, Cambridge University Press (1997).
- [7] D. Wohlleben, and B. Wittershagen, *Adv. Phys.* **34**, 403 (1985).
- [8] W. Franz, F. Steglich, W. Zell, D. Wohlleben, and F. Pobell, *Phys. Rev. Lett.* **45**, 64 (1980).
- [9] Y. Hiranaka, A. Nakamura, M. Hedo, T. Takeuchi, A. Mori, Y. Hirose, K. Mitamura, K. Sugiyama, M. Hagiwara, T. Nakama, and Y. Ōnuki *J. Phys. Soc. Jpn.* **82**, 083708 (2013).
- [10] Y. Luo, F. Ronning, N. Wakeham, X. Lu, T. Park, Z. -A. Xu, and J. D. Thompson, *Proc. Natl. Acad. Sci. USA* **112**, 13520 (2015).
- [11] S. Dzsaber, L. Prochaska, A. Sidorenko, G. Eguchi, R. Svagera, M. Wass, A. Prokofiev, Q. Si, and S. Paschen, *Phys. Rev. Lett.* **118**, 246601 (2017).

- [12] C. Y. Guo, F. Wu, Z. Z. Wu, M. Smidman, C. Cao, A. Bostwick, C. Jozwiak, E. Rotenberg, Y. Liu, F. Steglich, and H. Q. Yuan, *Nature Communications* **9**, 4622 (2018).
- [13] P.-Y. Chang, O. Erten, and P. Coleman, *Nature Phys.* **13**, 794 (2017).
- [14] K. Kuroda, M. Ochi, H. S. Suzuki, M. Hirayama, R. Noguchi, C. Bareille, S. Akebi, S. Kunisada, T. Muro, M. D. Watson, H. Kitazawa, Y. Haga, T. K. Kim, M. Hoesch, S. Shin, R. Arita, and T. Kondo, *Phys. Rev. Lett.* **120**, 086402 (2018).
- [15] T. Suzuki, *Physica B* **186-188**, 347 (1993).
- [16] H. Bartholin, P. Burllet, S. Quezel, J. Rossat-Mignod and O. Vogt, *J. Physique* **40**, C5 130 (1979).
- [17] H. Takahashi and T. Kasuya, *J. Phys. C: Solid State Phys.* **18**, 2697 (1985).
- [18] G.-J. Hu and B. R. Cooper, *Phys. Rev. B* **38**, 9127 (1988).
- [19] H. Kumigashira, S. -H. Yang, T. Yokoya, A. Chainani, T. Takahashi, A. Uesawa, T. Suzuki, O. Sakai, and Y. Kaneta, *Phys. Rev. B* **54**, 9341 (1996).
- [20] M. S. Litsarev, I. Di Marco, P. Thunström, and O. Eriksson, *Phys. Rev. B* **86**, 115116 (2012).
- [21] O. Sakai and Y. Shimizu, *J. Phys. Soc. Jpn.* **76**, 044707 (2007).
- [22] T. Kasuya, Y. S. Kwon, T. Suzuki, K. Nakanishi, F. Ishiyama, and K. Takegahara, *J. Magn. Mater.* **90&91**, 389 (1990).
- [23] T. Kasuya, Y. Hasa, Y. S. Kwon and T. Suzuki, *Physica B* **186**, 9 (1993).
- [24] G. Kresse and J. Hafner, *Phys. Rev. B* **47**, 558 (1993)
- [25] X. Duan, F. Wu, J. Chen, P. Zhang, Y. Liu, H. Q. Yuan, and C. Cao, *Commun. Phys.* **1**, 71 (2018).
- [26] F. Tran and P. Blaha, *Phys. Rev. Lett.* **102**, 226401(2009)

- [27] P. Li, Z. Z. Wu, F. Wu, C. Cao, C. Guo, Y. Wu, Y. Liu, Z. Sun, C. Cheng, D. S. Lin, F. Steglich, H. Q. Yuan, T. -C. Chiang, and Y. Liu, *Phys. Rev. B* **98**, 085103 (2018).
- [28] See Supplementary Materials.
- [29] S. Jang, R. Kealhofer, C. John, S. Doyle, J. Hong, Q. Si, O. Erten, J. D. Denlinger, and J. G. Analytis, *Sci. Adv.* **5**, eaat7158 (2019).
- [30] D. Ehm, S. Hübner, F. Reinert, J. Kroha, P. Wölfle, O. Stockert, C. Geibel, and H. V. Löhneysen, *Phys. Rev. B* **76**, 045117 (2007).
- [31] J. W. Allen, *J. Phys. Soc. Jpn.* **74**, 34 (2005).
- [32] J. H. Shim, K. Haule and G. Kotliar, *Science* **318**, 1615 (2007).
- [33] S.-K. Mo, W. S. Lee, F. Schmitt, Y. L. Chen, D. H. Lu, C. Capan, D. J. Kim, Z. Fisk, C. -Q. Zhang, Z. Hussain, and Z. -X. Shen, *Phys. Rev. B* **85**, 241103 (2012).
- [34] S.-I. Fujimori, Y. Saitoh, T. Okane, A. Fujimori, H. Yamagami, Y. Haga, E. Yamamoto, and Y. Ōnuki, *Nat. Phys.* **3**, 618 (2007).
- [35] Q. Y. Chen, D. F. Xu, X. H. Niu, J. Jiang, R. Peng, H. C. Xu, C. H. P. Wen, Z. F. Ding, K. Huang, L. Shu, Y. J. Zhang, H. Lee, V. N. Strocov, M. Shi, F. Bisti, T. Schmitt, Y. B. Huang, P. Dudin, X. C. Lai, S. Kirchner, H. Q. Yuan, and D. L. Feng, *Phys. Rev. B* **96**, 045107 (2017).
- [36] S. Jang, J. D. Denlinger, J. W. Allen, V. S. Zapf, M. B. Maple, J. N. Kim, B. G. Jang, and J. H. Shim, arXiv:1704.08247v1.
- [37] L. Moreschini, C. Dallera, J. J. Joyce, J. L. Sarrao, E. D. Bauer, V. Fritsch, S. Bobev, E. Carpena, S. Huotari, G. Vankó, G. Monaco, P. Lacovig, G. Panaccione, A. Fondacaro, G. Paolicelli, P. Torelli, and M. Grioni, *Phys. Rev. B* **75**, 035113 (2007).
- [38] K. Kummer, C. Geibel, C. Krellner, G. Zwicknagl, C. Laubschat, N. B. Brookes, and D. V. Vyalikh, *Nature Communications* **9**, 2011 (2018).

- [39] M. Sundermann, F. Strigari, T. Willers, H. Winkler, A. Prokofiev, J. M. Ablett, J. -P. Rueff, D. Schmitz, E. Weschke, M. M. Sala, A. A. Zein, A. Tanaka, M. W. Haverkort, D. Kasinathan, L. H. Tjeng, S. Paschen, and A. Severing, *Sci. Rep.* **5**, 17937 (2015).
- [40] J.-P. Rueff, S. Raymond, M. Taguchi, M. Sikora, J. -P. Itié, F. Baudelet, D. Braithwaite, G. Knebel, and D. Jaccard, *Phys. Rev. Lett.* **106**, 186405 (2011).

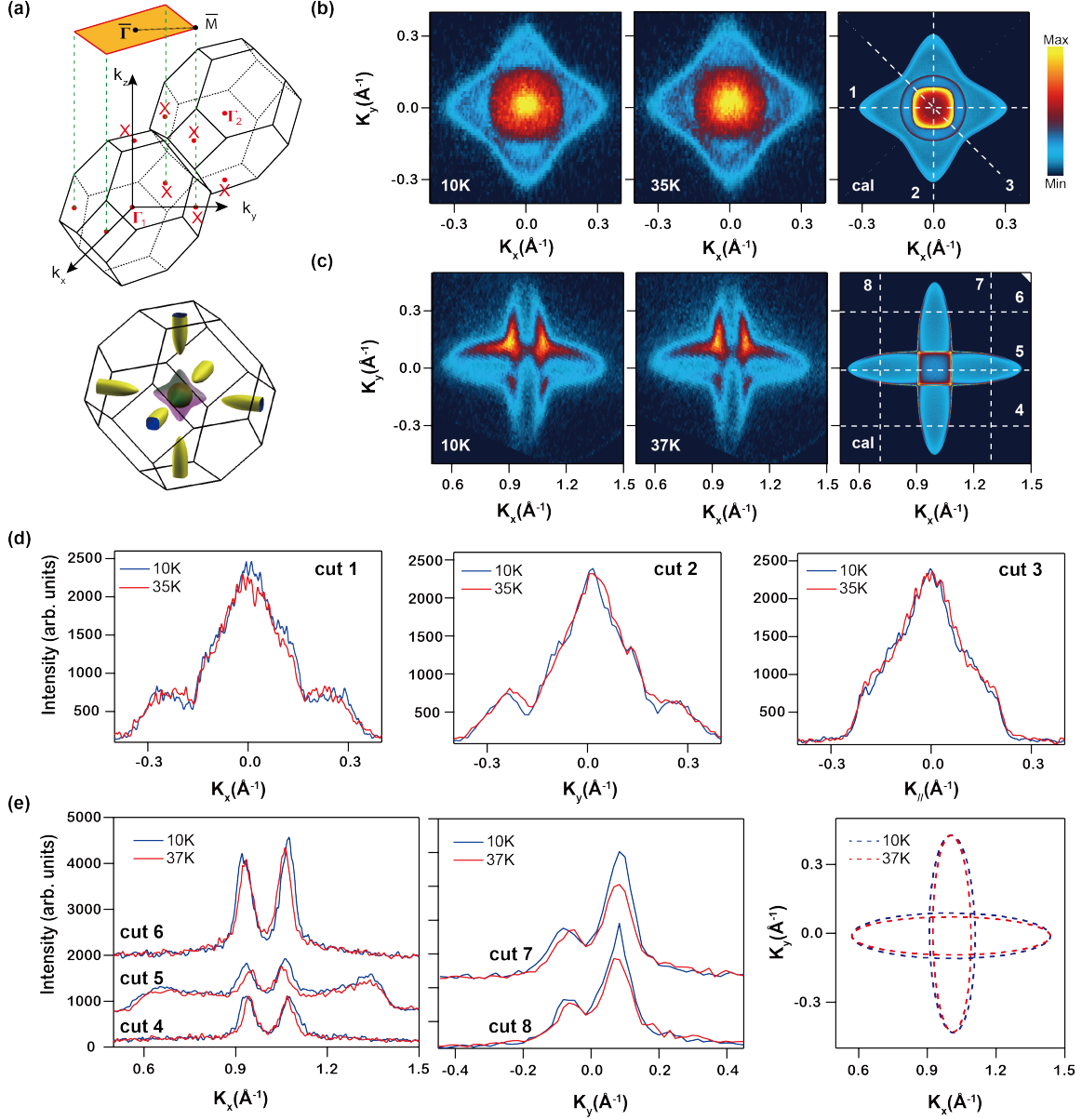


Fig. 1 (Color Online). Temperature-dependent FS of CeBi. (a) 3D and projected 2D BZs of CeBi (top), and the calculated 3D FS excluding Ce-4f electrons (bottom). (b,c) Experimental FS at 10 K and ~ 37 K (left and middle panels), in comparison with the DFT calculations (right panels, denoted by calc), for both the hole pocket near the $\bar{\Gamma}$ point (b) and the electron pocket near the \bar{M} point (c). The DFT calculations contain spectral contributions from all k_z 's in the 3D BZ, as well as a small energy broadening (0.001 eV). (d,e) MDC cuts for the hole (d) and electron (e) pockets. The cut directions are indicated in (b,c). The rightmost panel in (e) shows the extracted contour of the electron pocket at low and high temperatures.

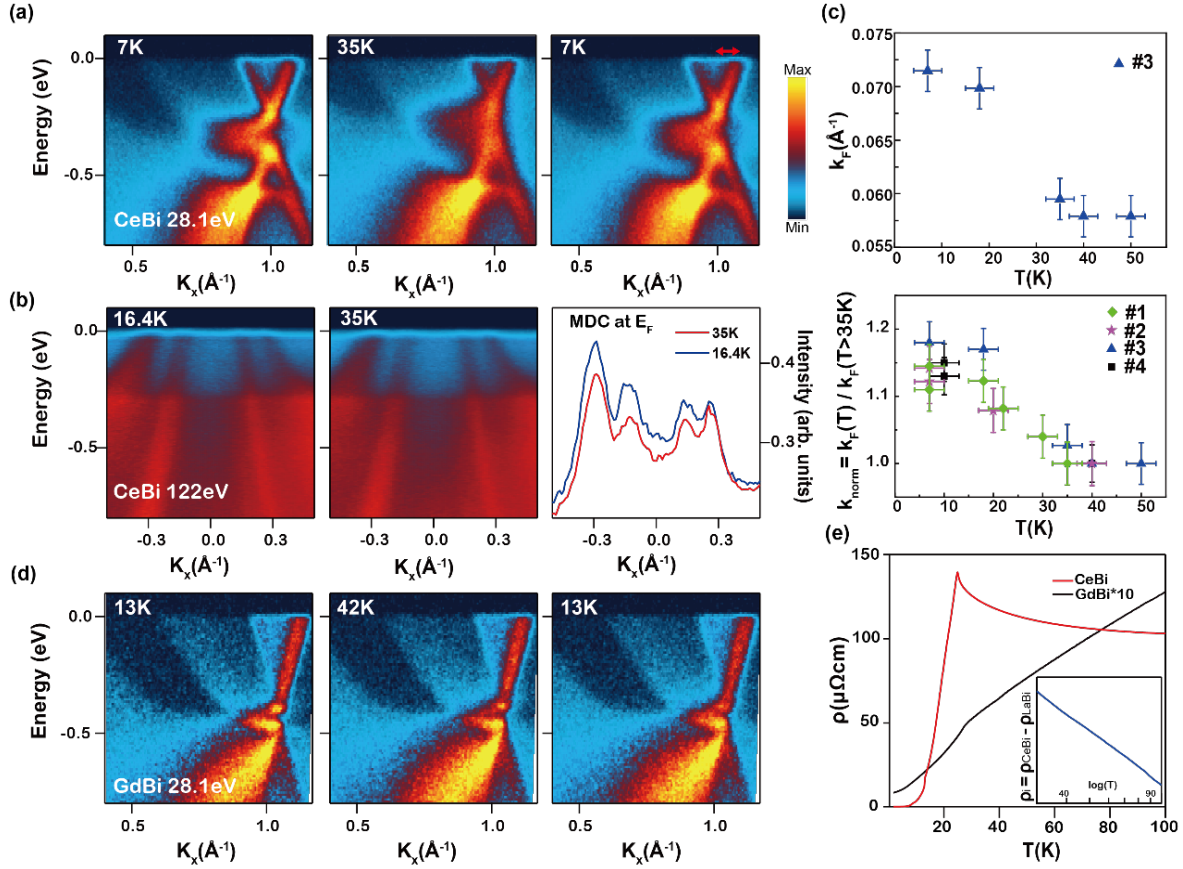


Fig. 2 (Color Online). Temperature evolution of the hole and electron pocket for CeBi, in comparison with GdBi. (a,b) temperature dependence of the energy-momentum cut for the electron (a) and hole (b) pocket. The data in (a) shows the evolution during a warming and cooling cycle from the same sample. The rightmost panel in (b) shows the MDC cuts at E_F ; no change in k_F can be observed. (c) Temperature evolution of k_F for the electron pocket (indicated by a red arrow in (a)). The top panel displays the raw data from a representative sample (#3), showing the onset of pocket expansion at ~ 35 K. The bottom panel summarizes the normalized Fermi vector $k_{\text{norm}} = k_F(T)/k_F(T > 35\text{K})$, for different samples. (d) Temperature evolution of the electron pocket for GdBi, showing no discernible change. (e) Resistivity vs temperature for CeBi and GdBi. The inset is the incremental part of the resistivity of CeBi, $\rho_i = \rho_{\text{CeBi}} - \rho_{\text{LaBi}}$, plotted as a function of $\log T$.

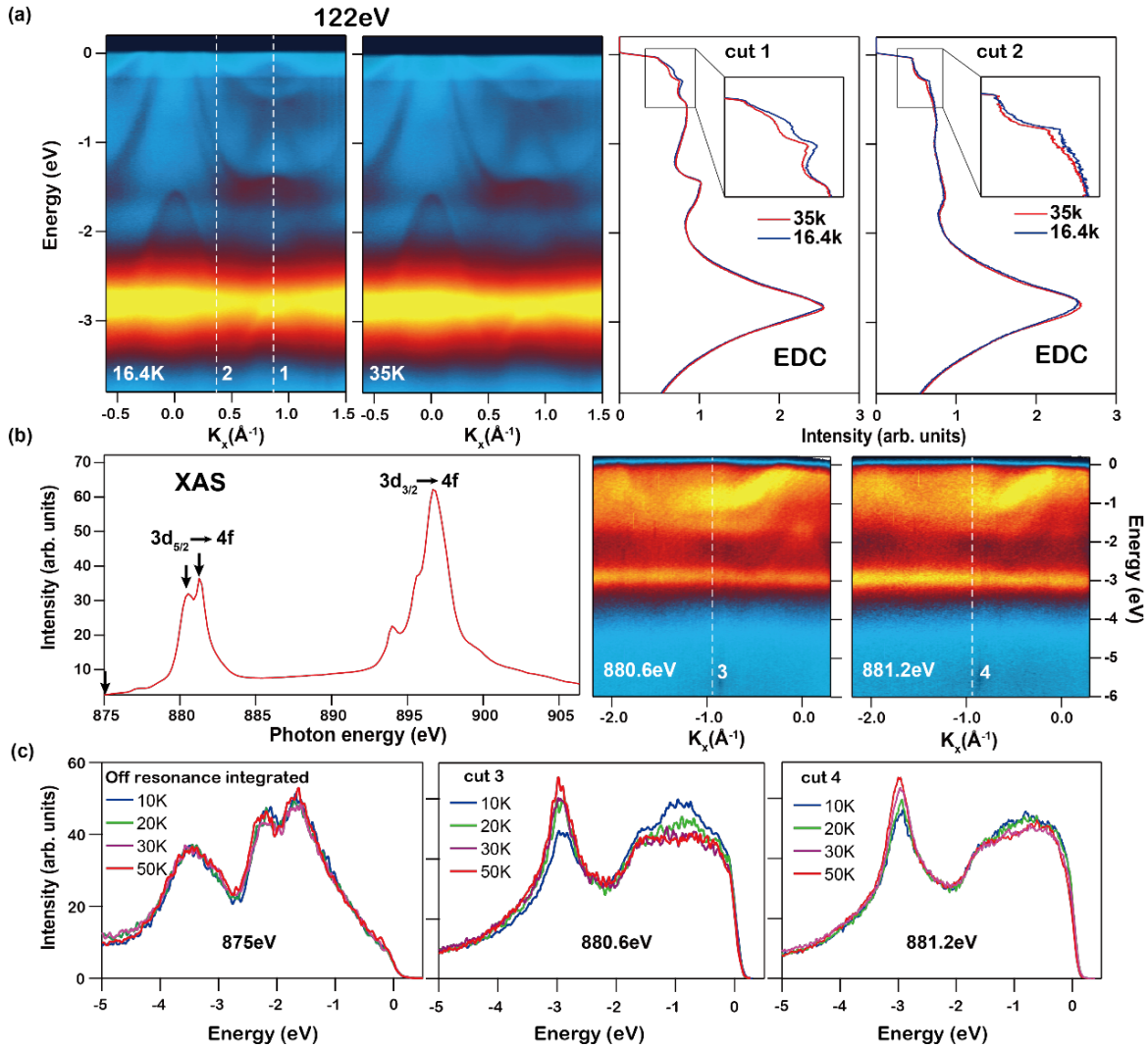


Fig. 3 (Color Online). Resonant ARPES results and temperature evolution. (a) Resonant ARPES results at Ce *N* edge (122 eV) at two representative temperatures. The EDC cuts at the hole and electron pockets are shown on the right panels, respectively. (b) Left: X-ray absorption spectroscopy (XAS) data near Ce *M* edge at 10 K. Right: Soft X-ray ARPES spectra taken at two representative photon energies (880.6 eV and 881.2 eV) at 10 K, indicated by black arrows in the XAS data. (c) Temperature dependence of EDCs at three representative photon energies (and momenta), indicated as white vertical lines in (b).

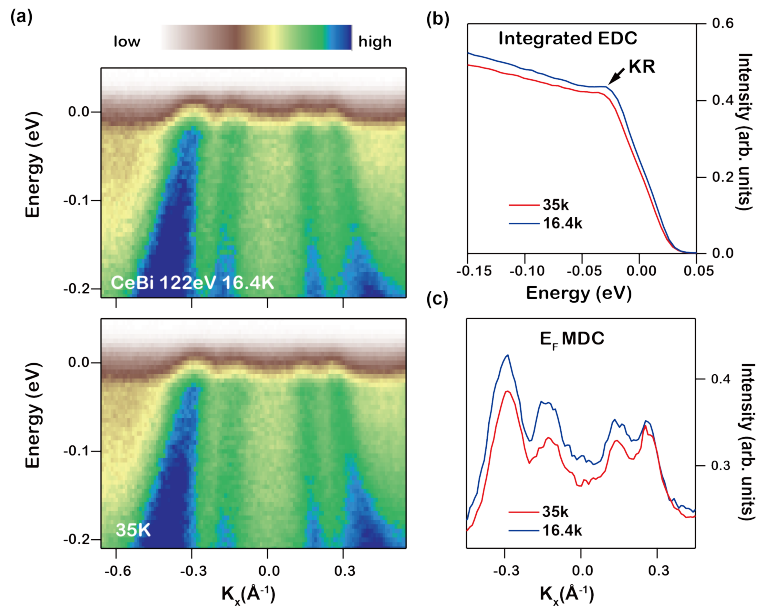


Fig. 4 (Color Online). (a) Zoom-in view of the ARPES spectra at the $\bar{\Gamma}$ point near E_F taken at two representative temperatures (the color bar is shown at the top). (b,c) Corresponding integrated EDC (b) and MDC at E_F (c).